Natural Hazards
https://doi.org/10.1007/s11069-024-06830-8

ORIGINAL PAPER

Ensemble modeling of extreme seasonal temperature trends in Iran under socio-economic scenarios

Muhammad Kamangar[1] · Mahmud Ahmadi[1] · Hamidreza Rabiei-Dastjerdi[2,4] · Zeinab Hazbavi[3]

Received: 26 January 2024 / Accepted: 12 July 2024

Abstract
In climate science, ensemble modeling has emerged as a powerful tool for addressing the uncertainties inherent in individual climate models. This approach generates more robust and reliable predictions by harnessing the collective insights of multiple models. Nonetheless, the method of combining these models to derive an ensemble model remains an open question. To this end, the objectives of this research are twofold: (i) to introduce and evaluate the weighted average-correlation ensemble model for projecting minimum and maximum temperatures in Iran, and (ii) to assess near-term (2021–2040) trends across 95 synoptic stations using socio-economic scenarios derived from five models: GFDL-ESM4, MPI-ESM1-2-HR, IPSL-CM6A-LR, MRI-ESM2, and UKESM1-0-LL. The ensemble technique effectively reduces the Root Mean Square Error (RMSE) (1/3 – 1/10) associated with the individual models. The predicted values for the minimum temperature are more similar to the actual data than the maximum temperature. The results also indicate a significant increase in the minimum temperature compared to the maximum temperature during the base period. The distribution of the maximum temperature across the country is influenced mainly by its latitude. In contrast, the distribution of the minimum temperature is influenced by both the country's major altitudes and latitudes. Surveys also indicate that, compared to the base period, there is an increasing trend in temperature for winter, spring, and autumn, while a decrease is observed during the summer. Notably, the increase in temperature is more pronounced during winter.

Highlights
- A new ensemble model was introduced and evaluated for projecting minimum and maximum temperatures in Iran.
- Trends in minimum and maximum temperatures in the near term (2021–2040) were obtained using socio-economic scenarios of five models at 95 synoptic stations.
- The ensemble technique reduced the error of the models used in projection to an optimal extent.

Keywords Climate change · Correlation · Ensemble · Taylor diagram · Temperature anomaly · Trend analysis

Extended author information available on the last page of the article

Published online: 14 August 2024

1 Introduction

Globally, climate change is an environmental issue of great concern that impacts the weather and climate extremes, such as low and high-temperature levels, precipitation, and runoff. For instance, global warming dramatically increases the intensity and duration of extreme weather and climate events (Perkins-Kirkpatrick and Gibson 2017; Hertel and Schlink 2019; IPCC 2023; Ashrafi et al. 2024). Previous research reported that climate change highly affects temperature extremes, highlighting its importance in climate change forecasts (e.g., Darand 2020; Das et al. 2023; Murali et al. 2023). The importance of climate forecasts at different national and international levels has recently increased as a scientific source for understanding climate change and evaluating its consequences in political and economic decisions (Hertel and Schlink 2019; IPCC 2023). Explicit forecasts with low uncertainty regarding the changes in precipitation and temperature from several months to decades provide significant consideration to model designers, experts, decision-makers, and policymakers (Hawkins and Sutton 2009; Stan and Xu 2014; Araghi et al. 2022; Yang and Tang 2023).

General Circulation Models (GCMs) are used to project climate parameters and study the effects of climate change. GCMs are three-dimensional models developed based on different climate scenarios to simulate the impact of greenhouse gases on Earth's climate and predict future changes. Using such models has limitations such as their incapability to render past climate efficiently, the high role of local factors (e.g., land cover and topography) in determining the climate of an area, structural error and uncertainty, and the adaptation of data with high spatial resolution to local climate data (Karl et al. 1990; Lupo et al. 2013). In addition, the direct climate model outputs (DMO) have uncertainty, and their bias must be removed before direct application to a specific area (Maraun 2016). Uncertainty of climate projection caused by (i) scenario: this type of uncertainty in different emission scenarios can be used as an external forcing for climate models; (ii) model response: this state is related to the response of different models to environmental conditions; (iii) natural variability: variability is the inherent behavior of the climate system and the resulting uncertainty can be seen in all models (Hawkins and Sutton 2009). The Coupled Model Intercomparison Project (CMIP) is a crucial action in inquiry on climate projections. It has been an influential resource to progress model advancement and methodical appreciation of the earth's structure by systematically comparing climate model outputs in different modeling hubs. Compared to the preceding versions, CMIP6 models, in addition to improving procedures and physical processes, have also considered novel criteria in the oceanic biogeochemistry and marine ice sectors (Hawkins and Sutton 2009; Zhu et al. 2020; Zarrin and Dadashi-Roudbari 2021; Das et al. 2023).

Various methods have been developed to remove the bias of climate models. However, there are many disagreements about using corrected outputs for studies related to the effects of climate change (Teutschbein and Seibert 2012; Maraun 2016; Ghafarian et al. 2022). Most bias removal methods are criticized for damaging the inherent advantages of models by changing the structure of temporal-spatial changes of variables and relationships between variables. In addition, all bias removal approaches, from simple scaling to more complex methods, are based on the assumption that the output bias of climate models is constant over time (Maraun 2016). It should be noted that even if bias removal can reduce the error from the output of climate models, no method can completely remove bias during a statistical cycle; this will be especially evident for long-term statistical periods (Chen

et al. 2013). Instead, the complexity of bias correction increases with the increase in the number of models, the number of variables, and the locations that must be corrected (Kim et al. 2023).

Using ten climate models, Chen et al. (2013) studied the limitations of removing bias in climate models. Their results showed the instability of the precipitation bias in the United States and Canada; in contrast, the temperature bias showed a constant value for both countries. Mendez et al. (2020) investigated the validity of six bias correction methods (BC), including the Delta Method (DT), Linear Scaling (LS), Rain Power Transform (PTR), Empirical Quantitative Mapping (EQM), Gamma Quantitative Mapping (GQM), and Gamma Pareto Quantitative Mapping (GPQM), and five climate models to remove the bias of monthly temperature predictions in Costa Rica. The results showed a significant reduction in error after applying the bias correction, and EQM and DT methods work much better than other methods. They stated that bias elimination directly affected the model performance, and the precipitation in Costa Rica showed a decreasing trend for the next period in the dry season. Kim et al. (2023) noted that most bias correction methods correct each variable independently, which leads to physical inconsistencies among variables. They have investigated the bias methods from simple to more complex techniques for correcting the biases of the Regional Climate Model (RCM) input boundary conditions. Their results showed that an RCM with multivariate bias correction, which corrects temporal continuity and relationships between variables, obtained extreme events better than univariate bias correction techniques, which do not consider the physical relationship between variables.

The importance of temperature and the effects of its change on the environment has caused many studies to be carried out. For example, Miao et al. (2014) examined temperature changes in northern Eurasia based on the Representative Concentration Pathway (RCP) scenarios of the Coupled Model Intercomparison Project (CMIP5) model. The results verified that in the 21st century, the temperature will escalate under all RCP scenarios. In addition, this escalation in temperature will accelerate with the increase in geographical latitude. Investigations showed that spring temperature will increase under RCP 2.6 and RCP 4.5 scenarios, and winter temperature will increase under the RCP 8.5 scenario. Zhu et al. (2017) investigated the changes in the extreme temperature in China based on RCP scenarios. They indicated a 6-degree increase in China's annual temperature until the end of the 21st century.

Zhu et al. (2020) investigated the changes in extreme temperatures under global warming. According to the results, a temperature increase is expected throughout the Indochina Peninsula and the Maritime Continent. Besides, there will be an increase in heat waves in the Philippines. Mao et al. (2021) examined the summer temperature anomaly in Antarctica under RCP scenarios. This investigation showed that temperature anomalies will increase during the period 2051–2099. Sun et al. (2021) also scaled the Loess Plateau precipitation for 30-year periods ending in 2050 and 2080 based on Vine Copula-Based Ensemble Downscaling (VCED). The results of this investigation indicated the optimality of the data obtained from the precipitation humidification. The surveys also showed a decrease in the annual precipitation in the south of the plateau and an increase in other parts. Yang and Tang (2023) microscaled the occurrence of prolonged hot and dry days in China. Their investigations showed that long-term hot and dry days will increase in most regions of China based on RCP 4.5 and RCP 8.5 scenarios. Furthermore, the spatial continuity of regions that experience long-term hot and dry days will increase significantly by the middle of the 21st century.

In Iran, Rezaei et al. (2015) measured the temperature in Kerman and Bam stations based on HadCM3 model output and A2 and B2 scenarios. They found that until 2099, the temperature will increase in all months of the year. Asakereh and Hesami (2019) also expected an increase in temperature in Isfahan Station until 2099. The results indicated a significant increase in the future climate's minimum and maximum daily temperature averages. Zarrin and Dadashi-Roudbari (2021) predicted Iran's near-term temperature using an ensemble CMIP6 multi-model approach. The results showed that the model ensemble with the independent weighted mean (IWM) method improves the projection of annual temperature, especially in arid and semi-arid regions.

In conclusion, Iran, with its extensive territory, is confronted with significant challenges arising from climate change, particularly evident in the alterations of temperature and precipitation patterns. These shifts in climate, as emphasized by Murali et al. (2023), have far-reaching consequences on both biological communities and the overall life-support systems of the planet. Therefore, it is essential to comprehend the intricate spatiotemporal distribution of these parameters, which forms the basis for the effective management of resources in the future. Despite significant progress in climate modeling, there are still inherent complexities in the Earth's climate system that give rise to uncertainties in temperature predictions. This study addresses this gap by introducing and evaluating the performance of a novel ensemble modeling approach for projecting the minimum and maximum temperatures in Iran under different socio-economic scenarios. By harnessing the collective power of diverse climate models, this research effectively reduces projection errors, providing a more robust foundation for informing decision-making in Iran in the near term.

2 Study area

Iran, located in southwest Asia, spans between latitudes 25° to 40° North, and longitudes 44° to 64° East, covering an area of 1,873,959 km^2 (Fig. 1). The country's territory includes numerous mountains above 4000 m in various regions with a mean elevation of over 1200 m above sea level. Due to the vastness of Iran's land, various geographical factors (e.g., latitude, tropical high pressure, and proximity to the seas), and its location at the junction of different atmospheric circulation systems, Iran experiences diverse climates (Najafi and Alizadeh 2023).

In terms of temperature, Iran can be alienated into cold mountainous and warm low-altitude regions. The mean temperature across the country is approximately 18 °C. The dominance of concurrent atmospheric systems, such as the Gange's low pressure and the Azore's high pressure, along with the atmosphere moisture content, create different temperature regions in Iran (Khoshakhlagh et al. 2008; Yadav 2016). The geographical distribution of temperature in summer is more homogeneous than in winter. The average annual precipitation is about 250 mm, which makes Iran one of the driest countries in the world (Kaboli et al. 2021). During the cold period (July to December), Iran experiences more precipitation due to the influence of western winds and contiguity to the moistness resource of the Mediterranean Sea (Ashrafi et al. 2024). However, in the warm times of the year, the impact of the Azores high pressure reduces precipitation. Precipitation in Iran is neither temporally nor spatially uniform. The southern shores of the Caspian Sea receive the highest precipitation, while the central deserts of Lut and the Salt Desert receive the lowest amount.

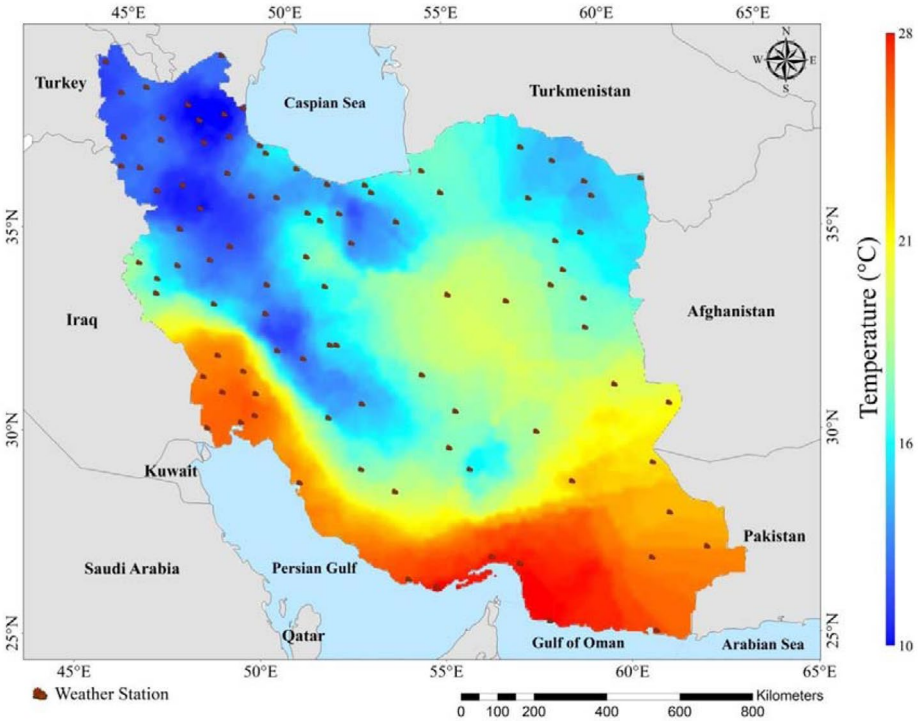

Fig. 1 Location of the study area and distribution of 95 synoptic stations

3 Research methodology

3.1 Data used and processing

Ground data (i.e., monthly minimum and maximum temperature) from 95 synoptic stations spanning from 1980 to 2014 have been utilized and analyzed as the reference period. In the station selection process, careful consideration was given to the diverse climatic regions of the country, with a focus on stations exhibiting minimal statistical gaps. "Gaps" refers to missing data points within the selected ground data sets for the synoptic stations that cover the reference period. These gaps can arise for different reasons, including equipment malfunction, human error during data collection, or natural events that disrupt observation capabilities. To ensure data quality, quantitative tests were conducted to investigate the outlier data, data homogeneity, and normality (Grubbs 1969; Alexandersson and Moberg 1997). A further analysis was also performed by aggregating the monthly data into seasonal values (winter, spring, summer, and autumn) spanning the entire reference period. This approach allows for exploring potential seasonal variations in temperature alongside the monthly analysis. The scattering of the studied ground stations is depicted in Fig. 1.

3.2 Coupled model intercomparison project phase six (CMIP6)

This study used five GCMs (MRI-ESM2, IPSL-CM6A-LR, UKESM1-0-LL, MPI-ESM1-2, and GFDL-ESM4) (Table 1). The MRI-ESM2 is a global climate model developed by Japan's Meteorological Research Institute (MRI) with moderate resolution. It employs a Geophysical Fluid Dynamics (GFD) system. Notable progress has been made compared to its predecessor, MRI-CGCM3, particularly in addressing issues like double-intertropical convergence and enhancing cloud representation (Kawai et al. 2019). In addition, The IPSL-CM6A-LR is a global climate model crafted by the Pierre-Simon Laplace Institute (IPSL) for investigating natural climate variability and climate responses to both natural and human-induced factors within the sixth phase of the CMIP6. This model is designed to simulate various aspects of the Earth's climate system, encompassing atmospheric, oceanic, and terrestrial processes, and has found extensive applications in studies such as the analysis of climate shifts over decades to multidecadal (Bonnet et al. 2021).

UKESM1-0-LL is a climate model utilized in phase 6 of the CMIP6 to simulate the Earth's climate system. It has been assessed for its capacity to depict the attributes and variety of the Antarctic Intermediate Water (AAIW) and its evolution under appropriate radiative forcing (Meuriot et al. 2023). MPI-ESM1-2 is also employed to replicate the Earth's climate system. This model encompasses parameters for the atmosphere, land surface, and sea ice and is applied in the study of an extensive array of topics related to climate, including atmospheric circulation patterns, hydrological behavior, water resources, and the repercussions of climate change and land use alterations (Ghassabi et al. 2023). Finally, the GFDL-ESM4 is a climate model that concentrates on the Earth system's inclusive interactions and is formulated by the Geophysical Fluid Dynamics Laboratory (GFDL). This model was produced based on advancements in component and coupled models during 2013–2018 for simulating carbon-chemistry-climate. It also achieved pivotal progress in dynamics and physics, taking into account airborne particles and their emissions, vegetation cover, terrestrial ecosystems, aerosols and fires, ecological and biogeochemical interactions in the ocean, and the interactive ocean-atmosphere cycle (Dunn et al. 2020).

The Earth System Models (ESMs) were used in this research. They are coupled climate models that explicitly model the movement of carbon in the Earth system. ESMs seek to simulate all relevant aspects of the Earth system, including physical, chemical, and bio-

Table 1 The models used to ensemble and project extreme temperatures

Model	Institution, country	Spatial resolution (degree)	Variant
MRI-ESM2	Meteorological Research Institute (MRI), Japan	1.25×1.25	r1i1p1
IPSL-CM6A-LR	institut pierre-simon laplace, France	2.50×1.26	r1i1p1
UKESM1-0-LL	Met Office Hadley Center, England	2.25×2.25	r1i1p1
MPI-ESM1-2-HR	Max Planck Institute, Germany	0.94×0.94	r1i1p1
GFDL-ESM4	Geophysical Fluid Dynamics Laboratory, America	1.25×1.00	r1i1p1

logical processes, thus far beyond their predecessors. The GCM shows the physics of the atmosphere and ocean.

In the selection of models, in addition to their availability and use in past research (e.g., GFDL-ESM4 by Sentman et al. (2018), IPSL-CM6A-LR by Boucher et al. (2020), MPI-ESM1-2-HR by Müller et al. (2018), and UKESM1-0-LL by Sellar et al. (2020), climate sensitivity is also considered. Climate sensitivity is usually defined as the increase in global temperature after a doubling of CO_2 concentration in the atmosphere compared to pre-industrial levels. Pre-industrial CO_2 was about 260 ppm, so its doubling will be about 520 ppm. There are different methods for defining climate sensitivity, depending on the time scales under consideration. Two of them are i- Transient Climate Response (TCR) - temperature increase at the moment when atmospheric carbon dioxide has doubled, which is defined as: "the change in the average temperature of the global surface, averaged over 20 years, focusing on the doubling time of atmospheric carbon dioxide, in the climate model simulation, with the assumption that atmospheric CO_2 concentration increases annually. This estimate is created using short-term simulations (typically 50–100 years) that allow for a focused analysis on the initial response of the climate system to a rapid CO_2 increase. While short-term simulations are valuable for understanding TCR, it is essential to acknowledge that they may not fully capture the long-term response of the climate system to sustained CO_2 increases (Bastiaansen et al. 2021).

3.3 Shared socio-economic pathways (SSPs)

A new set of climate scenarios, according to the sixth report of the IPCC, which has been improved in various ways, has led to the creation of climate change scenarios known as "Shared Socio-economic Pathways (SSPs)". SSPs are scenarios of projected changes in global socio-economic until the year 2100. They are utilized to extract greenhouse gas emission scenarios through diverse climate strategies. In this research, three scenarios of SSP1-2.6 (low emission and adaptation), SSP3-7.0 (middle scenario), and SSP5-8.5 (high emission and low adaptation) were used in the near term (2021–2040) (Haghighi et al. 2024). In this vein, first, the data of the models used in the closest points to the synoptic stations were extracted. Then, to unify the dimensions of the maps obtained from the models and the ground data, the ground data and the data extracted from the models were gridded. The Kriging method was used to grid the data. Nineteen kilometers was determined to be suitable for the dimensions of the pixels (19*19 km).

3.4 Validating the model output

Standard statistical criteria, including Root Mean Square Error (RMSE) and Percent Bias (PBIAS), were used to validate the direct model output (DMO). RMSE showed the standard deviation of the model in simulating the observed data, and the PBIAS indicated the percentage of the skewed value (Eqs. 1 and 2) (Ghafarian et al. 2022; Yeboah et al. 2022).

$$RMSE = \left[\frac{1}{N}\sum_{i=1}^{N}(X_{sim.i} - X_{obs.i})^2\right]^{1/2} \tag{1}$$

$$PBIAS = \left[\frac{\sum_{i=1}^{n} (X_{obs,\,i} - X_{sim,i}) \times 100}{\sum_{i=1}^{n} (X_{obs,i})} \right] \tag{2}$$

Where, $X_{sim.i}$ and $X_{obs.i}$ are the estimated and observed data. The closer RMSE and PBIAS is to zero, the higher the model's accuracy in estimating the desired variable. If the value of this measure tends to the positive side, it indicates that the desired variable is much lower than the actual estimated value. If it tends to the negative side, it indicates an overestimation of the variable by the model. No specific threshold has been considered for this parameter (Pervez and Henebry 2014).

3.5 Skew correction of projection models with the delta change factor (DCF)

To correct the skewness of the Decadal Climate Prediction Project (DCPP), the delta change factor (DCF) was used. The calculation description of the DCF method is given in Eq. (3):

$$\mathrm{T}_{\mathrm{fic}}^{\mathrm{BC}}(\mathrm{t}) = \mathrm{Te}_{\mathrm{obs}}(\mathrm{t}), \left[\frac{\mu_{\mathrm{m}} \mathrm{P}_{\mathrm{fic}}(\mathrm{t})}{\mu_{\mathrm{m}} \mathrm{P}_{\mathrm{contr}}(\mathrm{t})} \right] \tag{3}$$

Where, T is the desired variable; BC is the skew-corrected future projected time series; fic is the predicted future time series whose skewness should be corrected; Te specifically refers to the simulated minimum and maximum temperatures; obs is the observation period; t and μ_m are respectively time step and monthly long-term average; and contr is the number of simulated series of CMIP6-DCCP during the control period (Mendez et al. 2020).

3.6 The newly introduced ensemble method

A new model based on the weighted average correlation was used in projection to reduce the uncertainty of the models used in this research. The Eq. (4) was used to ensemble the data estimated by the models.

$$w^T x^j = \sum_{k=1}^{K} w_k x_k^i \tag{4}$$

Where, w_k is the weight of the data of each model, and x_k is the data estimated from the model. In this research, Pearson's correlation was used to determine the weight of the data. Pearson's correlation coefficient can be calculated from Eq. 5 (Pearson 1895).

$$r_{xy} = \frac{\sum_{i=1}^{N} (X_i - \overline{X})(Y_i - \overline{Y})}{\sqrt{\sum_{i=1}^{N} (X_i - \overline{X})^2 \sum_{i=1}^{N} (Y_i - \overline{Y})^2}} \tag{5}$$

Finally, each model that estimated data with a higher correlation with the actual data was assigned a higher weight. The following relationship was used to determine the weight.

$$w_k = \frac{r_k}{\sum_{k=1}^{K} r_k} \tag{6}$$

Where, r_k is the Pearson's correlation coefficient for each model.

3.7 Validation of ensemble model

Taylor's diagram was used to verify the DMO and validate climate models' output (Wehner 2013). It is based on the geometric relationship between correlation coefficient, standard deviation, and RMSE. Taylor's diagram is presented in two forms: a half circle showing negative and positive correlation and a quarter circle showing only positive correlation. In both cases, the values of the correlation coefficient are in the form of the radius of the circle on its arc, the values of the standard deviation are in the form of concentric circles concerning the reference point, and Root-mean-square deviations (RMSDs) are drawn as concentric circles concerning the center of the circle. The hollow circle on the horizontal axis of the reference point shows the ground station's location based on the time series's standard deviation. The location of any model closer to the reference point is more accurate (Wehner 2013).

The RMSD is used specifically to highlight the deviations squared and averaged from the center of the circle in Taylor's diagram, which can be different from RMSE which is typically used to express the prediction error of model outputs relative to actual values. Although both terms measure the average of the squared deviations, in Taylor's diagram, RMSD is specifically employed to show deviations relative to the center of the diagram (Hu et al. 2019).

3.8 Trend analysis

Non-parametric trend tests are methods without the necessity of having normal distributions, and they also have a high ability to monitor outlier data. The Mann-Kendall (M-K) test (Mann 1945; Kendall 1975) is among the most well-known non-parametric trend analyses. Mann-Kendall trend analysis has been increasingly used to detect trends in time series data (e.g., Sadeghi and Hazbavi 2015; Baghini et al. 2022; Li et al. 2022). The null hypothesis of this test is the randomness and the absence of a trend in the data series. Accepting the first hypothesis (null hypothesis) confirms the trend's existence in the data.

First, the difference between each observation and the others is calculated, and then the parameter S is calculated according to Eq. 7.

$$S = \sum_{k=1}^{n-1} \sum_{j=k+1}^{n} \operatorname{sgn}(x_j - x_k) \tag{7}$$

Where n is the number of observations, X_j and X_k show the jth and k^{th} values of the series, respectively. The sgn function is calculated as follows:

$$\operatorname{sgn}(x_j - x_k) = \begin{cases} +1 & if \quad (x_j - x_k) > 0 \\ 0 & if \quad (x_j - x_k) = 0 \\ -1 & if \quad (x_j - x_k) < 0 \end{cases} \tag{8}$$

The values of S and V(S) are used to compute the test statistic Z as follows:

$$Z = \begin{cases} x = \dfrac{S-1}{\sqrt{\operatorname{var}(s)}} \\ x = \dfrac{S+1}{\sqrt{\operatorname{var}(s)}} \end{cases} \qquad \begin{cases} if \quad S > 0 \\ if \quad S = 0 \\ if \quad S < 0 \end{cases} \tag{9}$$

If |Z| is larger than Zcrit, the null hypothesis is invalid, indicating that the trend is significant.

The magnitude of the trend can be estimated using the Sen's Slope/Theil–Sen estimator, a non-parametric method (Sen 1986). In this method, the median of the time series is used. The data is sorted in ascending order, and then the Sen's Slope value is obtained using Eq. 10:

$$f\ (1)\ =\ Qt\ +\ C\,(10)$$

Where C is a constant, and Q is the magnitude of the slope, which can be calculated from Eq. 11.

$$Q_{ij} = \frac{X_j - X_k}{j - k} \tag{11}$$

Where Q_{ij} is the Sen's Slope estimator from the median of the number of observations (N), and X_j and X_k are the data values in the time series.

The number of odd observations is obtained from Eq. 12, and the number of even observations is obtained from Eq. 13.

$$Q_{med} = Q\left(\frac{(N+1)}{2}\right) \tag{12}$$

$$Q_{med} = \frac{1}{2}\left(Q_{\left[\frac{N}{2}\right]} + Q_{\left[\frac{N+2}{2}\right]}\right) \tag{13}$$

Sen's Slope, a non-parametric statistic, relies on calculating the median of slopes between all possible pairs of data points. Its calculation for a dataset with an even number of observations requires a slightly different approach than an odd number of observations. This is because, with an even number of data points, the proper median slope might fall between two actual slopes in the data. Sen's Slope addresses this by averaging the slopes of the middle two data points (Sharma et al. 2019; Yagbasan et al. 2020).

A confidence interval is also calculated from the probability of determining whether the median slope is statistically different from zero using Eq. 14.

$$Ca = Z_{1-\frac{a}{2}}\sqrt{Var(s)} \tag{14}$$

Where, $Z_{1-\frac{a}{2}}$ is usually obtained from the standard normal distribution table.

4 Results and discussion

4.1 Validation of direct model output (DMO) of CMIP6

Validation of the temperature estimated by five models of GFDL-ESM4, MPI-ESM1-2-HR, IPSL-CM6A-LR, MRI-ESM2, and UKESM1-0-LL from the CMIP6 model series using stational data for the retrospective period (1991–2020) showed the RMSE between 1.4 and 10.8 in all investigated stations. The minimum and maximum estimated errors were observed in the UKESM1-0-LL and GFDL-ESM4. The maximum error in all five investigated models is observed in the northern half and the northeastern and western regions of the country (Fig. 2).

The error's low or high value can result from several factors, including the horizontal separation of models, sea-land interaction, and the lack of correct model estimation for the temperature variable. The ensemble model has provided higher efficiency than the other five models. However, it should be kept in mind that the RMSE is affected by the variable's value; therefore, it alone cannot be a suitable criterion for results validation. Another criterion called PBIAS was used along with RMSE to check the performance of the models. The PBIAS shows the percentage of temperature bias concerning the total temperature. PBIAS, unlike RMSE, is not affected by the variable's value (i.e., temperature).

Although the GFDL-ESM4 model has the highest RMSE values, this model has shown the lowest percentage of temperature bias (PBIAS) in the country. In general, the studied models estimate the temperature in Iran to be at least 28.7% lower than the actual value and, at most, 78.7% higher than the actual value. The low- and over-estimation in the projected

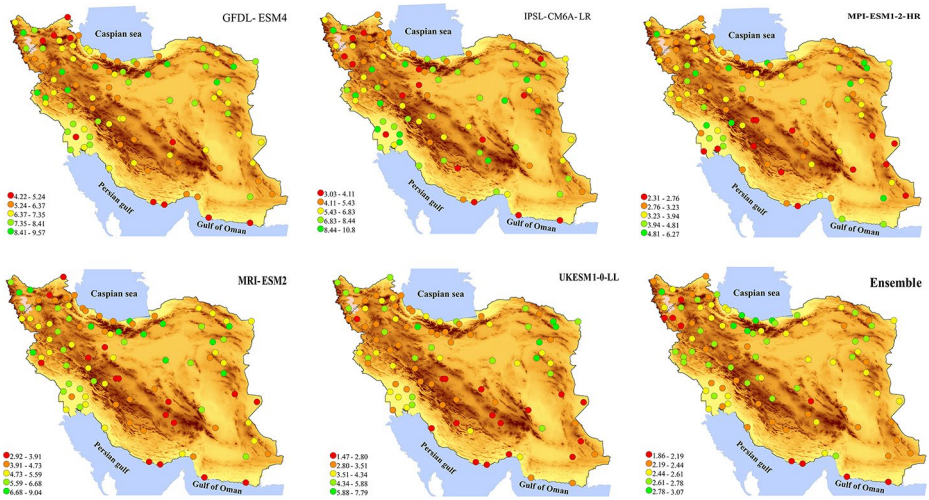

Fig. 2 Calculated error for maximum temperature based on RMSE

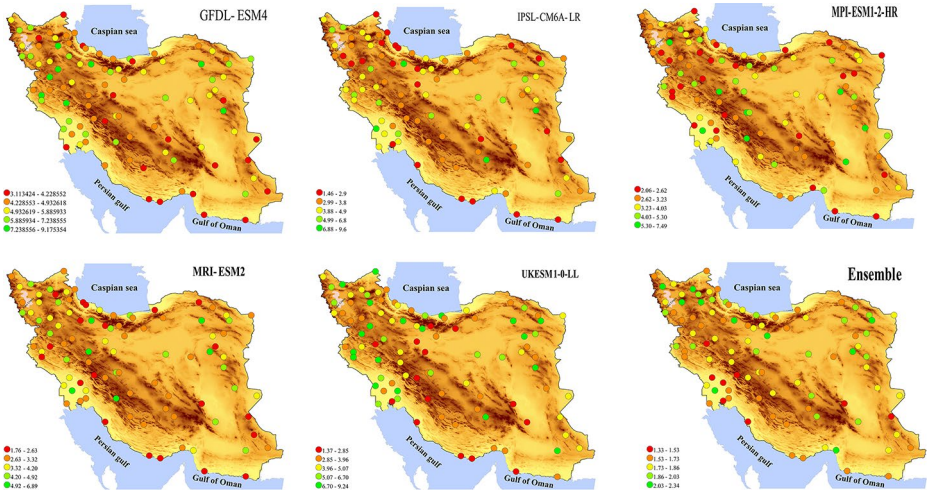

Fig. 3 Calculated error for minimum temperature based on RMSE

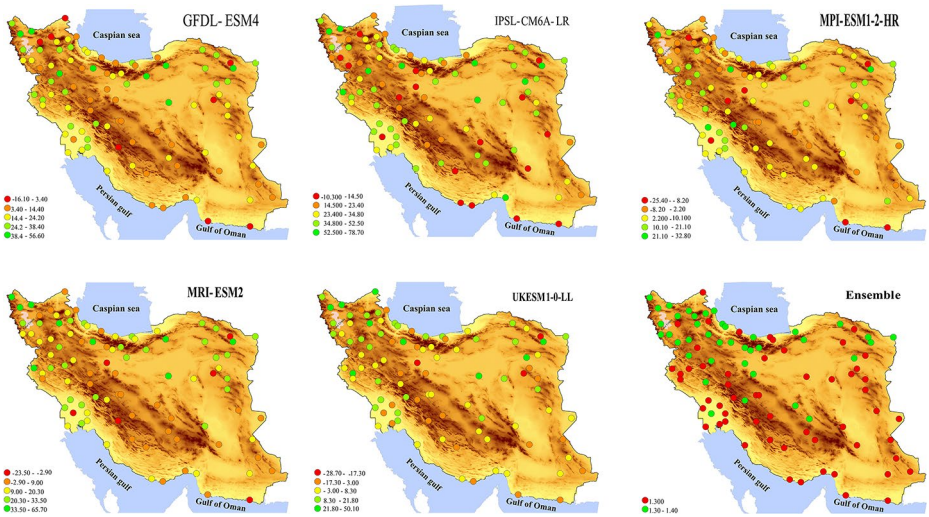

Fig. 4 Calculated error for maximum temperature based on PBIAS

data is 1 and 1.9%, respectively, which shows the ability of the method used to project the models.

Figures 2, 3, 4 and 5 show the maps resulting from applying the error criteria utilized to assess the simulated data accurately. It can be seen that each of the models in some parts of the country can estimate data with less error. For instance, some models have less error in areas with high altitudes, some in low-altitude areas, and others in coastal areas. This issue makes it necessary to compare the data obtained from different models. It can be seen that the error of the simulated data with the ensemble model is much less than in other models (Figs. 2, 3, 4 and 5).

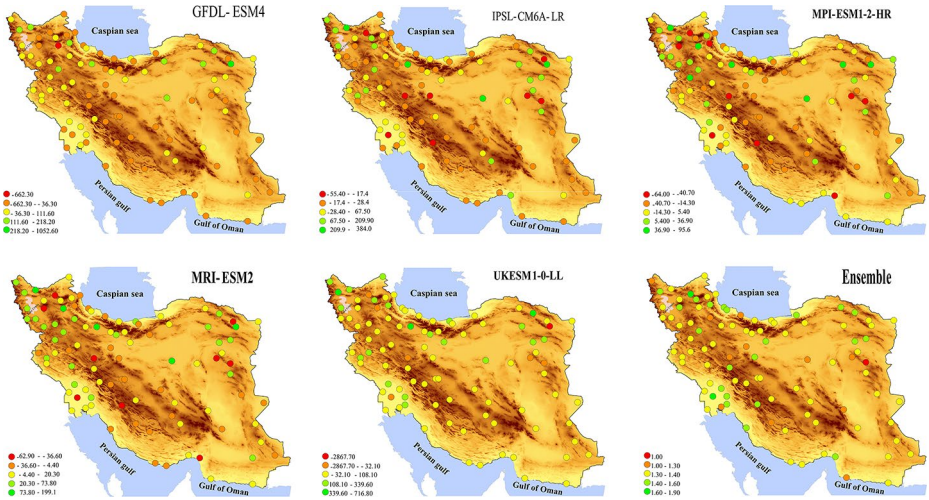

Fig. 5 Calculated error for minimum temperature based on PBIAS

4.2 Validation of CMIP6-DCPP bias-corrected models

A general examination of the Taylor diagram shows that the ensemble model produced from the five mentioned models correlates more with the observational data. The ensemble model has shown a high correlation of 0.8 with the observational data, significantly increasing its efficiency compared to individual models. In addition, the ensemble model has presented a lower standard deviation than individual models.

Examining the validation results of individual models with Taylor's diagram showed that in the winter season, the MPI-ESM1-2-HR and MRI-ESM2-0 models; in the autumn and spring seasons, the MRI-ESM2-0 model and in the summer season, the MPI-ESM1-2-HR have better efficiency. The results showed that the efficiency of the ensemble model in estimating seasonal precipitation has increased compared to individual models corrected for skewness in the central areas of Iran (Figs. 6 and 7).

4.3 Distribution of maximum temperature during the period 2021–2040

The maximum temperature distribution in the base and near-term seasons based on the used scenarios has been shown in Fig. 8. In the base period, the temperature has been increasing in the winter season from the northwest to the southeast of the country. The same trend will be maintained in the near term. Nevertheless, the temperature has increased in all three scenarios compared to the base period. In the spring and summer seasons, the spatial trend of the maximum temperature in the base and near term in all three scenarios is similar to winter. The only difference is the location of the maximum temperature, which has been moved to the southwest of the country. The northwestern highlands also experience low temperatures, like in the winter season. Of course, the extent of the minimum temperature areas has decreased compared to the spring season. In this season, the southwest of the country experiences the highest temperatures. Of course, the size of this area will be smaller

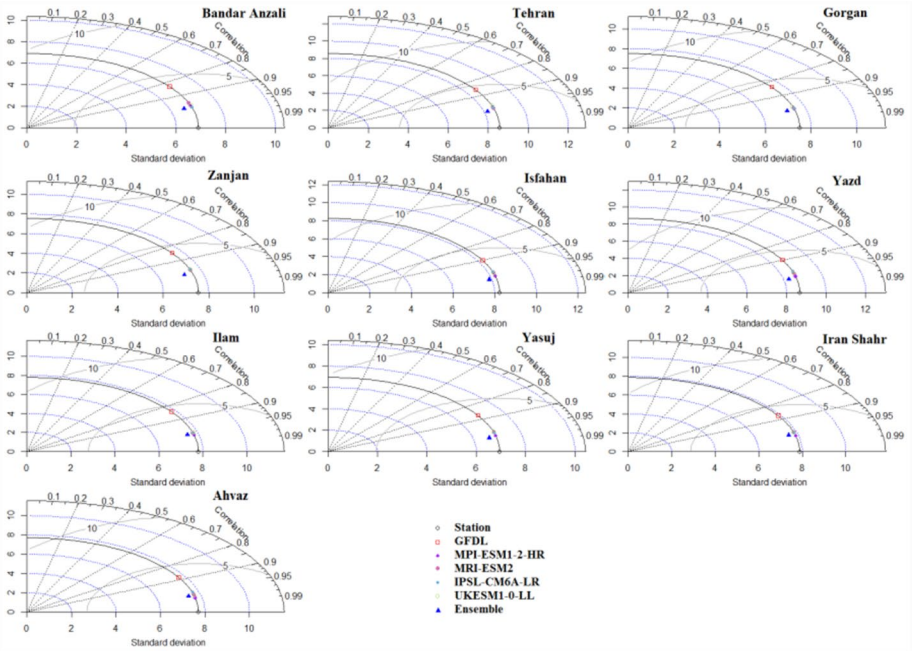

Fig. 6 Taylor diagram for ten selected stations for minimum temperature

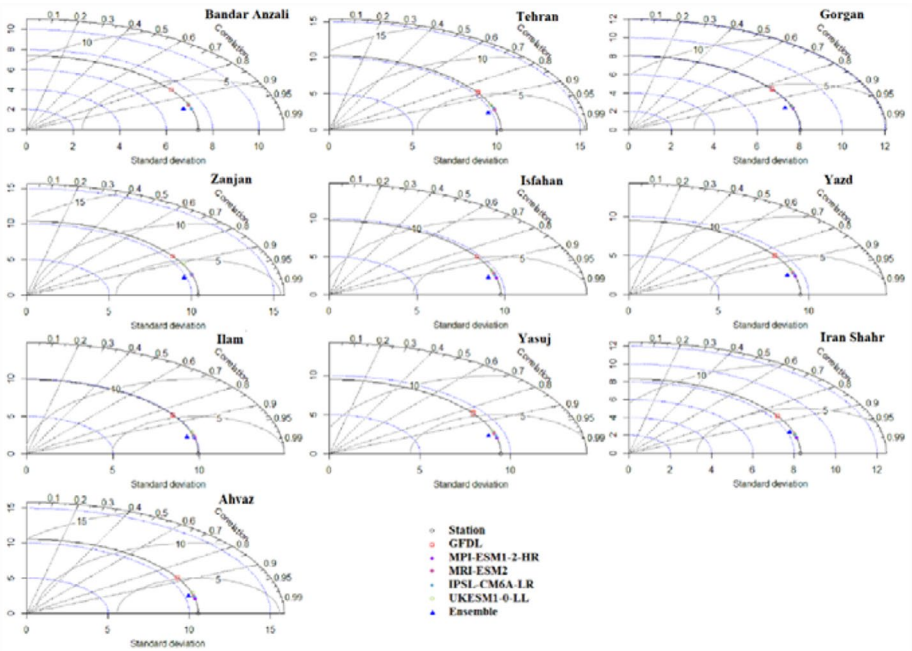

Fig. 7 Taylor diagram for ten selected stations for maximum temperature

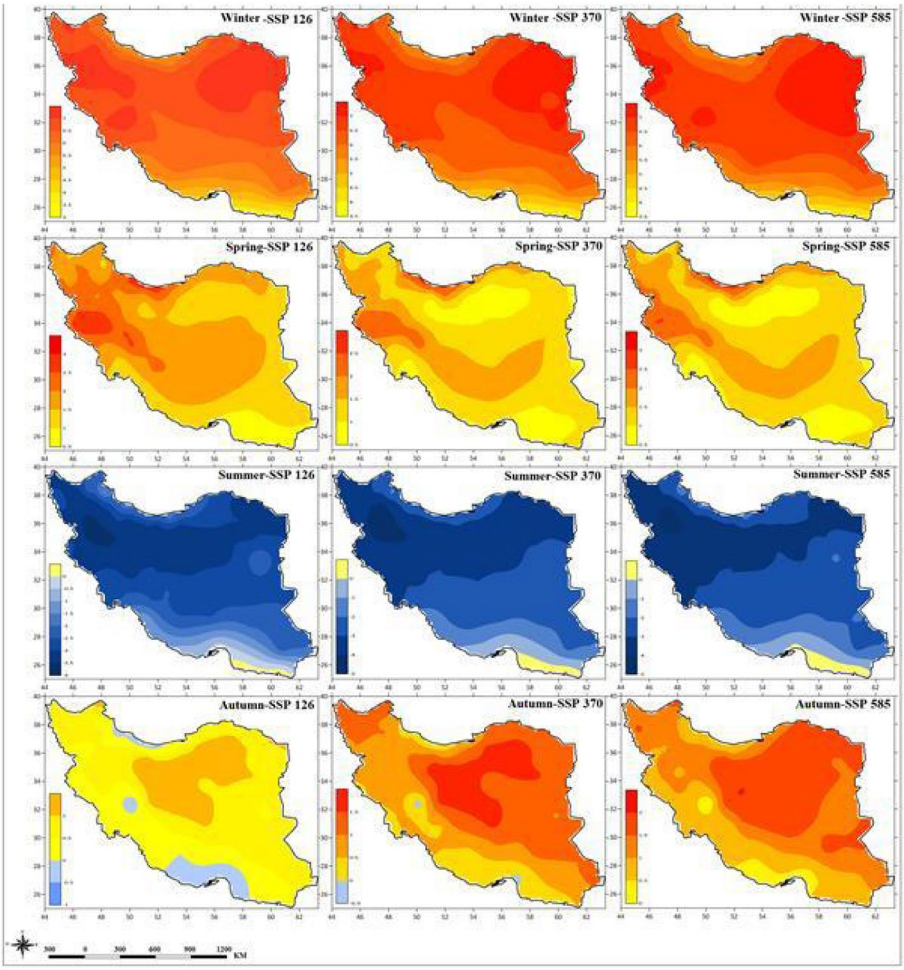

Fig. 8 Maximum temperature anomaly in the seasons in the near term (2021–2040) based on SSP scenarios compared to the base period

in the near term compared to the base period. One of the remarkable things in this season is the relative uniformity in the warm central areas.

In the autumn season, the areas of maximum temperature have moved from the southwest of the country to the south in the east of the Strait of Hormuz. The extent of the maximum area in the base period and the SSP1-2.6 scenario is more significant. All the northwest and then the heights of Zagros and Alborz experience lower temperatures. Based on the scenarios used in this research, the temperature will increase in the winter and spring seasons compared to the base period in the near term. This increase is more severe in the winter season, and in some areas of the country, such as the east and western parts, it will reach up to 7 °C. In the southern regions, the increase in temperature in winter and spring will be lower than in other parts of the country. In the summer season, the temperature in the near term is predicted to be lower than the base period. In other words, we will face cooler

summers in the next two decades. A slight increase in temperature is expected only on the coast of the Oman Sea. In the northwestern highlands of the country, the temperature will decrease more than in other places. In autumn, the situation is slightly different. So, in the SSP1-2.6 scenario, the temperature will decrease in some parts of the country and increase in a large part. In the SSP 370 and SSP5-8.5 scenarios, the temperature will increase.

By examining the temperature anomaly maps in the near term, it was found that the winter season is the most different from the temperature in the base period. The most negligible difference can be seen in the autumn season. The study of Zarrin and Dadashi-Roudbari (2021) also indicated an increased temperature in the near term (2021–2040).

4.4 Distribution of minimum temperature during the period 2021–2040

Figure 9 shows the distribution of the minimum temperature in the seasons in the base and the near term based on the planned scenarios. The seasonal distribution of the minimum temperature in winter is similar to the maximum temperature. In this way, the temperature increases from the northwest to the southeast of the country. The northwest of the country and part of the Zagros highlands experience lower temperatures than other parts. The highest temperatures are also seen on the coasts of Oman. An interesting point is the temperature equality of part of the Caspian coast with the central regions. These areas have a higher temperature than their surroundings. The higher night temperature on the Caspian coast is due to the presence of more humidity in the atmosphere of this region because the humidity in the atmosphere affects temperature regulation and moderates the coldness of the air.

In spring, the spatial behavior of night temperature is similar to winter, with the difference that the area of the small areas in the northwest of the country has been reduced. Besides, the extent of the hot central areas has increased. In this season, the highest temperatures can be seen on the coasts of Oman. Relatively high temperatures also occur in other parts of the southern coasts. The night temperature has increased in summer compared to spring. The northwest, parts of the Zagros highlands, parts of the northeast, and scattered spots in the country's center experience minimum night temperatures. All the southern coasts of the country continuously have the highest night temperatures. In this season, the Caspian coast has higher temperatures than its surroundings. The temperature of this area is equal to that of the central part of the country.

In the autumn season, the extent of the minimum temperature areas in the northwest has increased compared to the summer and has extended to the southern parts of Zagros. The maximum temperatures are also limited to the coasts of the Oman Sea. For minimum temperatures, like the maximum temperature, an increased trend is expected in the near term in the winter and spring seasons compared to the base period. The increase in minimum temperature will be more severe in winter. In the northern half of the country, the increase in temperature in winter and spring is higher than in other parts of the country. In the summer season, the minimum temperature in the near term is predicted to be lower than the base period. In other words, cooler nights are expected in the near term in the summer season. In autumn, the situation is slightly different. So, in the SSP1-2.6 scenario, the temperature will decrease on the shores of the Caspian Sea and increase in other parts of the country. In the other two scenarios, the temperature will increase. By examining the minimum temperature anomaly maps in the near term, it was found that the winter season has the most significant difference with the temperature in the base period (Fig. 9). Our study confirmed that the

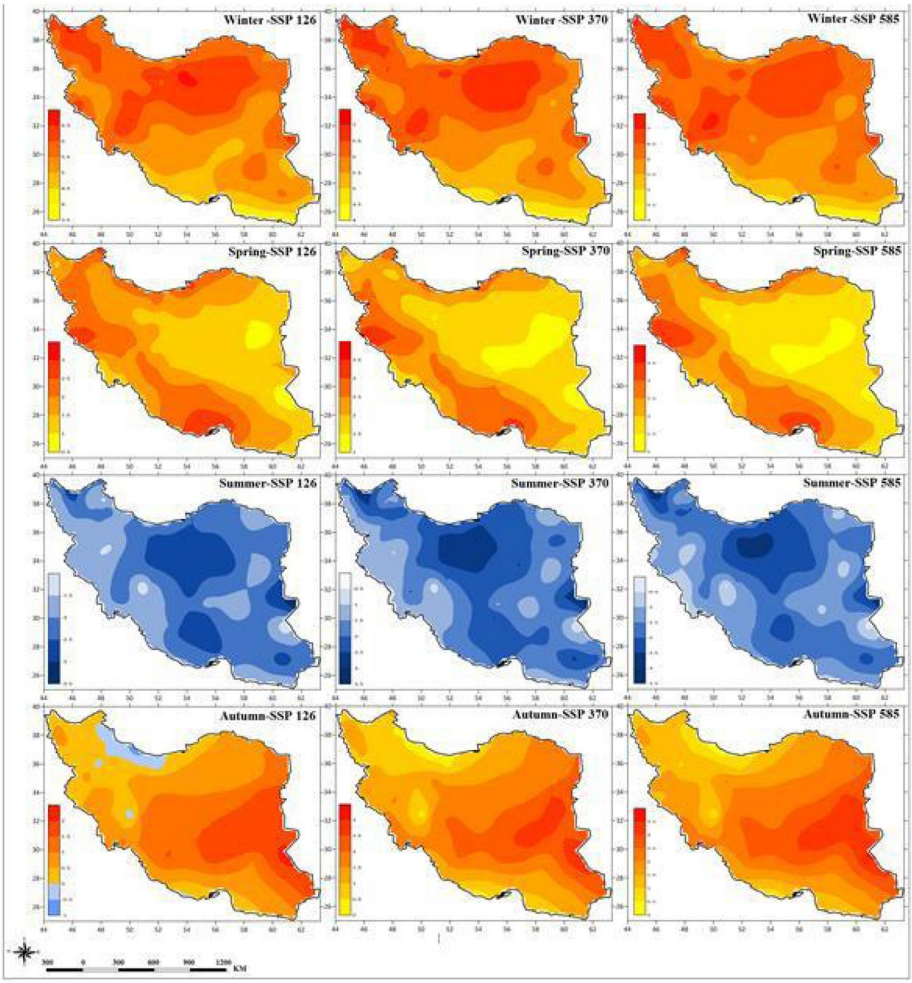

Fig. 9 Minimum temperature anomaly in the seasons in the near term (2021–2040) based on SSP scenarios compared to the base period

limitations of observed weather data could be overcome using gridded temperature datasets. Araghi et al. (2022) also demonstrate the effectiveness of gridded temperature datasets in crop simulation modeling for agricultural applications and consequently address the data scarcity challenges. However, further research is needed to examine the performance of gridded datasets in diverse agro-climatic zones.

4.5 Seasonal trends of maximum temperature during the period 2021–2040

The seasonal trend of maximum temperature during the near term for different scenarios is shown in Fig. 10 (only the stations with a significant trend are considered). In the winter, an increasing trend can be seen in all scenarios. This increasing trend will be more intense at higher altitudes. In spring, according to the SSP1-2.6 scenario, there is a decrease in Zagros,

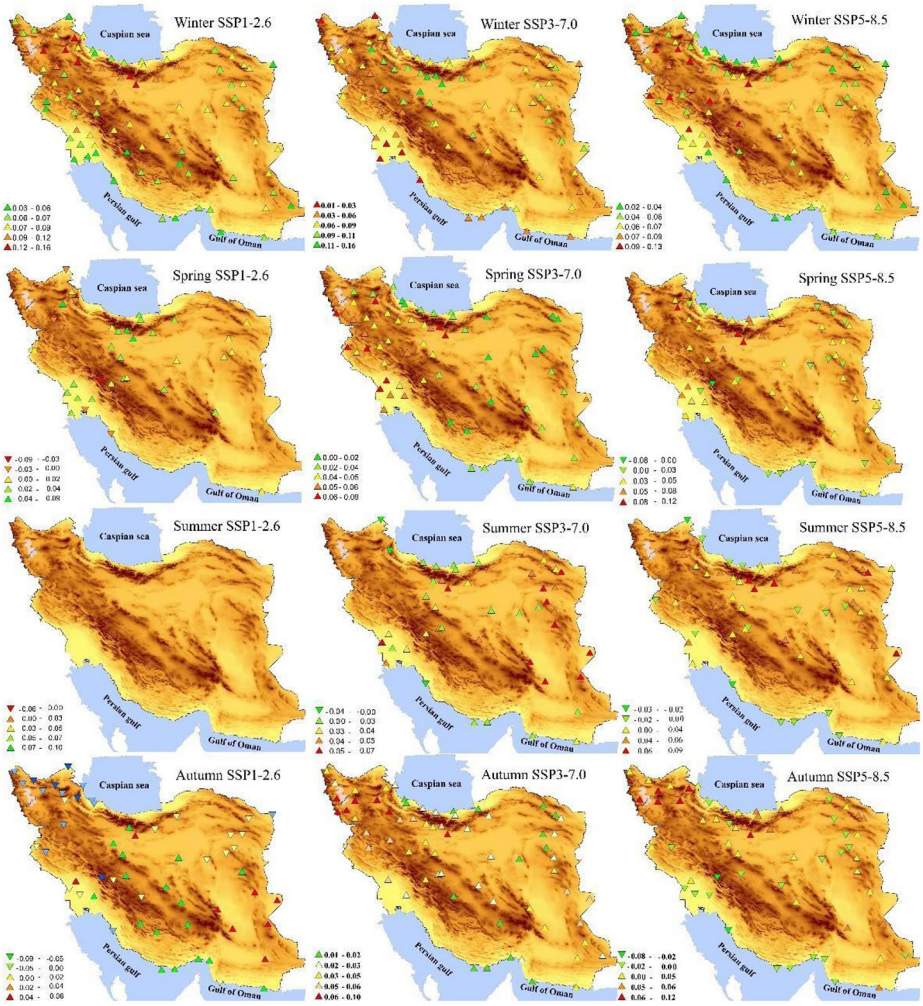

Fig. 10 Seasonal trend of maximum temperature in the near term (2021–2040)

west and northwest of the country, and an increase in other places. The country's eastern, southeastern, and southern coasts do not have significant trends. In the SSP 370 scenario, the whole country will have an increasing trend. The increasing trend will be stronger in the west and northwest and Alborz. In the SSP5-8.5 scenario, there is a decreasing trend in the northeast, east, parts of Zagros, and the southwestern coasts of the Caspian, and an increasing trend prevails in other parts of the country. In the summer season, there was no significant trend in the SSP1-2.6 scenario of the whole country.

In the SSP 370 scenario, a decreasing temperature trend is seen only in the highlands of Talesh, and other parts of the country experience an increasing trend. The increasing trend is more intense in the east of the country. The northwestern and western parts of the country have not had a significant trend either. In the scenario of SSP5-8.5, there is a decreasing trend in the southwestern coasts of the Caspian, the southern coasts of the country, and parts

of the center, and an increasing trend in other parts. In the autumn season, an increasing trend can be seen in the SSP1-2.6 scenario in the southeast, southern coasts, and the center of the country. Temperature trends are decreasing in the northwest, northeast, and eastern Alborz. In the SSP 370 scenario, the whole country has an increasing trend. The northwest of the country experiences a more substantial increase. In the SSP5-8.5 scenario, a decreasing trend can be seen in the northeast, southwest, center, and southern coast, and an increasing trend in other parts of the country. In the northwest of the country, the increasing trend is more intense. The winter season will generally experience the most severe temperature increase (Fig. 10).

4.6 Seasonal trend of minimum temperature during the period 2021–2040

The seasonal trend of minimum temperature during the near term for different scenarios has been shown in Fig. 11 (only the stations with a significant trend are considered). In the winter season, according to the SSP1-2.6 scenario, there is an increasing trend in some areas, such as the eastern, central, and northwestern parts of the country, and a decreasing trend in the west, southwest, and coasts of Oman. In the SSP 370 and SSP5-8.5 scenarios, all stations in the country will have an increasing trend. In the spring season, according to the scenarios of SSP1-2.6 and SSP 370, there will be a decreasing trend in most of the eastern, central, and some areas of the Caspian coast, and an increasing trend will prevail in the highlands of the northwest, some parts of Zagros, the west and the southwest.

In the scenario of SSP5-8.5, most of the country's regions have an increasing trend, and a decreasing trend can be seen scattered in some parts. In the summer season, according to the SSP1-2.6 scenario, the east, southwest, parts of the center, and parts of the Caspian coast have an increasing trend, and the northwest, Zagros, and northeast of the country have a decreasing trend. According to the SSP 370 scenario, the east, northeast, southwest, west, northwest, and parts of the center will have an increasing trend, and the Caspian coasts and parts of the center will have a decreasing trend.

In the SSP5-8.5 scenario, the east, center, parts of Zagros, and northeast will increase, and the Caspian coast, southern Zagros, west, and parts of the northwest will have a decreasing trend. In the autumn season, according to the SSP1-2.6 scenario, large parts of the northwest, Zagros, and southwest of the country have a decreasing trend. An increasing trend can be seen in the east, southeast, and parts of the country's center. The northern coasts of the country have not had a significant trend. In the SSP 370 scenario, there is a decrease in large parts of the country, and only in parts of the northwest and central highlands, there is an increasing trend. In the SSP5-8.5 scenario, an increasing trend will occur in most parts of the country. The decreasing trend can be seen weakly in small and scattered parts, such as the center and northwest. The most robust increasing trend will be in winter and autumn based on the SSP5-8.5 scenario (Fig. 11).

5 Conclusion

The minimum and maximum temperature of 95 synoptic stations were modeled and generated for the baseline period (1985–2014) and near term (2021–2040) using socio-economic scenarios of five models (GFDL-ESM4, MPI-ESM1-2-HR, IPSL-CM6A-LR, MRI-ESM2,

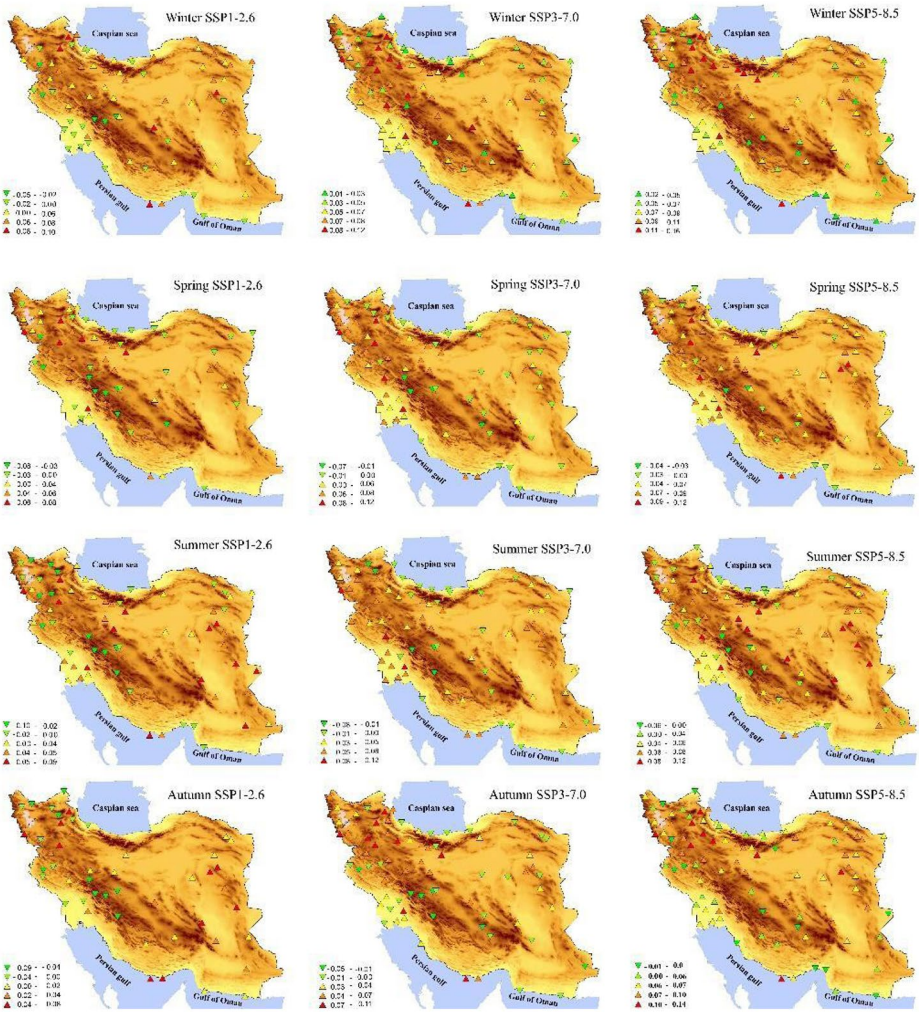

Fig. 11 Seasonal trend of minimum temperature in the near term (2021–2040)

and UKESM1-0-LL). In addition, the new ensemble model was introduced and evaluated based on the correlation of model output with stational data. The introduced method was used with the weighted average method for the ensemble, and the Pearson correlation method was used to determine the models' weight. The error calculation showed that the accuracy of the used models reduces the error of the models to an acceptable level. Accordingly, the weighted average-correlation ensemble model effectively reduced the error in temperature projections, demonstrating its potential for accurate climate change projections. Investigations of temperature anomalies showed that during 2021–2040, the minimum and maximum temperatures will increase in most parts of the country. According to the projections, the main centers of temperature increase will be concentrated in the southwest and south of Iran. Moreover, examining the temperature trend in the near term shows the trend (increasing and decreasing) in the minimum and maximum temperature in most regions of

the country. The increasing trend in the main highlands of the country has been more intense than in other areas. The winter will have the most robust increasing trend in temperature compared to the base period.

Since climate change impacts various sectors of society, including agriculture, water resources, and human health, examining the extracted trends in this research could be a sound basis and assist decision-makers in different sectors in developing adaptation strategies for human-environment systems protection. As developed in our research, the weighted-average correlation model is just one of several possible combination models. Therefore, we should compare our results with the performance of other homogeneous methods, such as Bayesian Model Averaging (BMA) and Simple Model Averaging (SMA), to determine which model performs best for projecting the minimum and maximum temperatures and trends.

Acknowledgements We would like to thank the Iran Science Foundation (ISF) for its generous support of this research. Finally, we would like to thank our families and friends for their love and support.

Author contributions Muhammad Kamangar: Study design, Data preprocessing, Methodology, Visualization, Writing draft. Mahmud Ahmadi: Study design, Supervision. Hamid Rabiei: Writing draft, Reviewing, and editing. Zeinab Hazbavi: Methodology, Writing draft, Reviewing, and editing. All authors read and approved the final manuscript.

Funding Open Access funding provided by the IReL Consortium. Open access funding provided by School of Architecture, Planning and Environmental Policy & CeADAR, University College, Dublin, Ireland. Additionally, the ISF grant (No. 40025) provided the funding that made this work possible. The authors have no relevant financial or non-financial interests to disclose.
Open Access funding provided by the IReL Consortium

Data availability This study used data from the Iran Meteorological Organization and the Sixth Scenario Model. The Iran Meteorological Organization data are free from the Iran Meteorological Organization website (https://data.irimo.ir/). The Sixth Scenario Model data are available through the Climate Modeling Engineering Network (ESGF) (https://esgf-node.llnl.gov/search/cmip6/). Data processing and analysis were performed using QGIS, R, and RStudio software. The versions of the software used in this study are as follows: QGIS: Version 3.32.2 Lima (https://www.qgis.org/en/site/) R: Version 4.2.3 (https://www.r-project.org/) RStudio Desktop: Version 2023.09.0+463 (https://posit.co/download/rstudio-desktop/).

Conflict of interests The authors have no relevant financial or non-financial interests to disclose.

References

Alexandersson H, Moberg A (1997) Homogenization of Swedish temperature data. Part I: homogeneity test for linear trends. Int J Climatol 17:25–34. https://doi.org/10.1002/(SICI)1097-0088(199701)17:1%3C25::AID-JOC103%3E3.0.CO;2-J

Araghi A, Martinez C, Olesen J, Hoogenboom G (2022) Assessment of nine gridded temperature data for modeling of wheat production systems. Comput Electron Agric 199:107189. https://doi.org/10.1016/j.compag.2022.107189

Asakereh H, Hesami N (2019) Assessing the application of artificial neural networks and SDSM models to simulate the minimum and maximum temperatures at Isfahan Station. J Geogr Res Desert Areas 6(2):133–158. https://doi.org/10.29252/grd.2018.1476(In Persian)

Ashrafi S, Karbalaee AR, Kamangar M (2024) Projections patterns of precipitation concentration under climate change scenarios. Nat Hazard 1–14

Baghini N, Falahatkar S, Hassanvand MS (2022) Time series analysis and spatial distribution map of aggregate risk index due to tropospheric NO2 and O3 based on satellite observation. J Environ Manage 304:114202. https://doi.org/10.1016/j.jenvman.2021.114202

Bastiaansen R, Dijkstra HA, von der Heydt AS (2021) Multivariate estimations of equilibrium climate sensitivity from short transient warming simulations. Geophys Res Lett 48. https://doi.org/10.1029/2020GL091090. :e2020GL091090

Bonnet R, Boucher O, Deshayes J, Gastineau G, Hourdin F, Mignot J et al (2021) Presentation and evaluation of the IPSL-CM6A-LR ensemble of extended historical simulations. J Adv Model Earth Syst 13:e2021MS002565. https://doi.org/10.1029/2021MS002565

Boucher O, Servonnat J, Albright AL, Aumont O, Balkanski Y, Bastrikov V et al (2020) Presentation and evaluation of the IPSLCM6A- LR climate model. J Adv Model Earth Syst 12(7): e2019MS002010

Chen J, Brissette FP, Chaumont D, Braun M (2013) Finding appropriate bias correction methods in downscaling precipitation for hydrologic impact studies over North America. Water Resour Res 49(7):4187–4205. https://doi.org/10.1002/wrcr.20331

Darand M (2020) Future changes in temperature extremes in climate variability over Iran. Meteorol Appl 27:e1968. https://doi.org/10.1002/met.1968

Das S, Islam ARMT, Kamruzzaman M (2023) Assessment of climate change impact on temperature extremes in a tropical region with the climate projections from CMIP6 model. Clim Dyn 60(1–2):603–622. https://doi.org/10.1007/s00382-022-06416-9

Dunn RJ, Alexander LV, Donat MG, Zhang X, Bador M, Herold N et al (2020) Development of an updated global land in situ-based data set of temperature and precipitation extremes: HadEX3. J Geophys Res-Atmos 125(16):e2019JD032263. https://doi.org/10.1029/2019JD032263

Ghafarian F, Wieland R, Lüttschwager D, Nendel C (2022) Application of extreme gradient boosting and Shapley additive explanations to predict temperature regimes inside forests from standard open-field meteorological data. Environ Model Softw 156:105466. https://doi.org/10.1016/j.envsoft.2022.105466

Ghassabi Z, Fattahi E, Habibi M (2023) Variability in future atmospheric circulation patterns in the MPI-ESM1-2-HR model in Iran. Atmosphere 14:307. https://doi.org/10.3390/atmos14020307

Grubbs F (1969) Procedures for detecting outlying observations in samples. Technometrics 11(1):1–21

Haghighi P, Soleimanpour SM, Moradi A (2024) The effects of climate change on precipitation and temperature using SSP scenarios (case study: Fars province). https://doi.org/10.22098/mmws.2024.14691.1425. Water Soil Manage Model

Hawkins E, Sutton R (2009) The potential to narrow uncertainty in regional climate predictions. Bull Am Meteorol Soc 90(8):1095–1108. https://doi.org/10.1175/2009BAMS2607.1

Hertel D, Schlink U (2019) Decomposition of urban temperatures for targeted climate change adaptation. Environ Model Softw 113:20–28. https://doi.org/10.1016/j.envsoft.2018.11.015

Hu Z, Chen X, Zhou Q, Chen D, Li J (2019) DISO: a rethink of Taylor diagram. Int J Climatol 39:2825–2832. https://doi.org/10.1002/joc.5972

IPCC (2023) Climate change 2023: Synthesis report. Contribution of Working Groups I, II, and III to the sixth Assessment Report of the Intergovernmental Panel on Climate Change [Core Writing Team, H. Lee and J. Romero (eds.)]. IPCC, Geneva, Switzerland, 184 pp. https://doi.org/10.59327/IPCC/AR6-9789291691647

Kaboli S, Hekmatzadeh AA, Darabi H, Haghighi AT (2021) Variation in physical characteristics of rainfall in Iran, determined using daily rainfall concentration index and monthly rainfall percentage index. Theor Appl Climatol 144:507–520. https://doi.org/10.1007/s00704-021-03553-9

Karl TR, Wang WC, Schlesinger ME, Knight RW, Portman D (1990) A method of relating general circulation model simulated climate to the observed local climate. Part I: Seasonal statistics. J Clim 3(10):1053–1079. https://doi.org/10.1175/1520-0442(1990)003%3C1053:AMORGC%3E2.0.CO;2

Kawai H, Yukimoto S, Koshiro T, Oshima N, Tanaka T, Yoshimura H, and Nagasawa R (2019) Significant improvement of cloud representation in the global climate model MRI-ESM2. Geosci Model Dev 12:2875–2897. https://doi.org/10.5194/gmd-12-2875-2019

Kendall MG (1975) Rank correlation methods, fourth edn. Charles Griffin, London

Khoshakhlagh F, Ouji R, Jafarbeglou M (2008) A synoptic study on seasonal patterns of wet and dry spells in Midwest of Iran. Desert 13(2):89–103. https://doi.org/10.22059/jdesert.2008.36293

Kim Y, Evans JP, Sharma A (2023) Multivariate bias correction of regional climate model boundary conditions. Clim Dyn 61:3253–3269. https://doi.org/10.1007/s00382-023-06718-6

Li J, He S, Wang J, Ma W, Ye H (2022) Investigating the spatiotemporal changes and driving factors of nighttime light patterns in RCEP Countries based on remote sensed satellite image. J Clean Prod 359:131944. https://doi.org/10.1016/j.jclepro.2022.131944

Lupo A, Kininmonth W, Armstrong JS, Green K (2013) Global climate models and their limitations. Clim Change Reconsidered II: Phys Sci 9:148. http://weather.missouri.edu/gcc/_09-09-13_%20Chapter%201%20Models.pdf

Mann HB (1945) Non-parametric test against trend. Econometrika 13:245–259. https://doi.org/10.2307/1907187

Mao R, Kim SJ, Gong DY et al (2021) Increasing difference in interannual summertime surface air temperature between Interior East Antarctica and the Antarctic Peninsula under future climate scenarios. Geophys Res Lett 48(16):e2020GL092031. https://doi.org/10.1029/2020GL092031

Maraun D (2016) Bias correcting climate change simulations- A critical review. Curr Clim Change Rep 2(4):211–220. https://doi.org/10.1007/s40641-016-0050-x

Mendez M, Maathuis B, Hein-Griggs D, Alvarado-Gamboa L-F (2020) Performance evaluation of bias correction methods for climate change monthly precipitation projections over Costa Rica. Water 12(2):482. https://doi.org/10.3390/w12020482

Meuriot O, Lique C, Plancherel Y (2023) Properties, sensitivity, and stability of the Southern Hemisphere salinity minimum layer in the UKESM1 model. Clim Dyn 60:87–107. https://doi.org/10.1007/s00382-022-06304-2

Miao C, Duan Q, Sun Q et al (2014) Assessment of CMIP5 climate models and projected temperature changes over Northern Eurasia. Environ Res Lett 9(5):055007. https://doi.org/10.1088/1748-9326/9/5/055007

Müller WA, Jungclaus JH, Mauritsen T, Baehr J, Bittner M, Budich R et al (2018) A higher-resolution version of the Max Planck Institute Earth System Model (MPI-ESM1. 2-HR). J Adv Model Earth Syst 10(7):1383–1413. https://doi.org/10.1029/2017MS001217

Murali G, Iwamura T, Meiri S, Roll U (2023) Future temperature extremes threaten land vertebrates. Nature 615(7952):461–467. https://doi.org/10.1038/s41586-022-05606-z

Najafi MS, Alizadeh O (2023) Climate zones in Iran. Meteorol Appl 30(5):e2147. https://doi.org/10.1002/met.2147

Pearson K (1895) VII. Note on regression and inheritance in the case of two parents. Proc Royal Soc Lond 58(347–352):240–242. https://doi.org/10.1098/rspl.1895.0041

Perkins-Kirkpatrick SE, Gibson PB (2017) Changes in regional heatwave characteristics as a function of increasing global temperature. Sci Rep 7:12256. https://doi.org/10.1038/s41598-017-12520-2

Pervez MS, Henebry GM (2014) Projections of the Ganges–Brahmaputra precipitation-downscaled from GCM predictors. J Hydrol 517:120–134. https://doi.org/10.1016/j.jhydrol.2014.05.016

Rezaei M, Nahtani M, Abkar A, Rezaei M, Mirkazehi Rigi M (2015) Performance evaluation of statistical downscaling model (SDSM) in forecasting temperature indexes in two arid and hyper arid regions (Case study: Kerman and bam). Water Soil 5(10):117–131. https://doi.org/10.22067/jsw.v0i0.23119

Sadeghi SHR, Hazbavi Z (2015) Trend analysis of the rainfall erosivity index at different time scales in Iran. Nat Hazard 77:383–404. https://doi.org/10.1007/s11069-015-1607-z

Sellar AA, Walton J, Jones CG, Wood R, Abraham NL, Andrejczuk M et al (2020) Implementation of UK Earth system models forCMIP6. J Adv Model Earth Syst 12(4). https://doi.org/10.1029/2019MS001946. e2019MS001946

Sen PK (1986) Estimates of the regression coefficient based on Kendall's tau. J Am Stat Assoc 63:1379–1389. https://doi.org/10.1080/01621459.1968.10480934

Sentman LT, Dunne JP, Stouffer RJ, Krasting JP, Toggweiler JR, Broccoli AJ (2018) The mechanistic role of the Central American Seaway in a GFDL Earth System Model. Part 1: impacts on global ocean mean state and circulation. Paleoceanogr Paleoclimatol 33(7):840–859. https://doi.org/10.1029/2018PA003364

Sharma D, Kumar B, Chand S (2019) A trend analysis of machine learning research with topic models and Mann-Kendall Test. Int J Intel Syst Appl 11(2):70–82. https://doi.org/10.5815/ijisa.2019.02.08

Stan C, Xu L (2014) Climate simulations and projections with a super-parameterized climate model. Environ Model Softw 60:134–152. https://doi.org/10.1016/j.envsoft.2014.06.013

Sun C, Huang G, Fan Y, Zhou X, Lu C, Wang X (2021) Vine copula ensemble downscaling for precipitation projection over the Loess Plateau based on high-resolution multi-RCM outputs. Water Resour Res 57:e2020WR027698. https://doi.org/10.1029/2020WR027698

Teutschbein C, Seibert J (2012) Bias correction of regional climate model simulations for hydrological climate-change impact studies: review and evaluation of different methods. J Hydrol 456:12–29. https://doi.org/10.1016/j.jhydrol.2012.05.052

Wehner M (2013) Very extreme seasonal precipitation in the NARCCAP ensemble: model performance and projections. Clim Dyn 40(1):59–80. https://doi.org/10.1007/s00382-012-1393-1

Yadav RK (2016) On the relationship between Iran surface temperature and northwest India summer monsoon rainfall. Int J Climatol 36:4425–4438. https://doi.org/10.1002/joc.4648

Yagbasan O, Demir V, Yazicigil H (2020) Trend analyses of meteorological variables and lake levels for two shallow lakes in Central Turkey. Water 12(2):414. https://doi.org/10.3390/w12020414

Yang Y, Tang J (2023) Downscaling and uncertainty analysis of future concurrent long-duration dry and hot events in China. Clim Change 76:11. https://doi.org/10.1007/s10584-023-03481-9

Yeboah KA, Akpoti K, Kabo-bah AT, Ofosu EA, Siabi EK, Mortey EM, Okyereh SA (2022) Assessing climate change projections in the Volta Basin using the CORDEX-Africa climate simulations and statistical bias-correction. Environ Chall 6:100439. https://doi.org/10.1016/j.envc.2021.100439

Zarrin A, Dadashi-Roudbari A (2021) Projected changes in temperature over Iran by 2040 based on CMIP6 multi-model ensemble. Phys Geog Res 53(1):75–90. https://doi.org/10.22059/jphgr.2021.308361.1007551(In Persian)

Zhu J, Huang G, Wang X, Cheng G (2017) Investigation of changes in extreme temperature and humidity over China through a dynamical downscaling approach. Earth's Future 5:1136–1155. https://doi.org/10.1002/2017EF000678

Zhu S, Ge F, Fan Y, Zhang L, Sielmann F, Fraedrich K, Zhi X (2020) Conspicuous temperature extremes over Southeast Asia: seasonal variations under 1.5°C and 2°C global warming. Clim Change 160:343–360. https://doi.org/10.1007/s10584-019-02640-1

Authors and Affiliations

Muhammad Kamangar[1] · Mahmud Ahmadi[1] · Hamidreza Rabiei-Dastjerdi[2,4] · Zeinab Hazbavi[3]

✉ Hamidreza Rabiei-Dastjerdi
hamid.rabiei@ucd.ie

Muhammad Kamangar
Mohamad.kamangar63@gmail.com

Mahmud Ahmadi
mahmudahmadi1344@gmail.com

Zeinab Hazbavi
z.hazbavi@uma.ac.ir

1 Department of Climatology, Faculty of Earth Sciences, Shahid Beheshti University, Tehran, Iran

2 School of Architecture, Planning and Environmental Policy & CeADAR (Ireland's National Centre for Applied Data Analytics & AI), University College, Dublin, Ireland

3 Department of Range and Watershed Management, Faculty of Agriculture and Natural Resources and Member of Water Management Research Center, University of Mohaghegh Ardabili, Ardabil, Iran

4 Social Determinants of Health Research Center, Isfahan University of Medical Sciences, Isfahan, Iran